Supplementary Material

April 13, 2016

1 Making the micro-rods

Tripartite rods (Au-Pt-Au) were synthesized by electrochemical deposition using an Anodized Aluminum Oxide (AAO) membrane as template. The method reported in the literature [1], was modified to avoid hydrogen evolution upon the deposition of gold on platinum segment. A 150 nm thick silver film was deposited on an AAO membrane (GE healthcare, Whatman, product No.6809-5522, 47 mm diameter, 0.2μm pore size) by thermal evaporation (0.1-0.15 nm/s, Leica microsystems Inc., Bal-Tec Med 020). The membrane was placed in a home-made Teflon electrochemical cell with the silver-coated side facing an aluminum foil that was used as a working contact. Ag/AgCl electrode (CH Instruments Inc.) and a platinum mesh were used as a reference and a counter electrode, respectively.

All the electrodes were connected to a potentiostat (CH Instruments Inc., CHI440A) to perform electrochemical deposition. Ag buffer layer was deposited at -1 V from an aqueous solution of silver cyanide (0.0185 M, AgCN, Thermo Fisher Scientific Inc.), potassium pyrophosphate (0.3027 M, K4P2O7, Sigma-Aldrich Co. LLC.), and potassium cyanide (0.1228 M, KCN, Thermo Fisher Scientific Inc.) [2]. The first Au layer was deposited at -0.92 V from a commercial plating solution (Technic Inc., OROTEMP 24 RTU), and the Pt layer was deposited at -0.4 V from an aqueous solution of ammonium hexachloroplatinate (0.010 M, (NH4)2PtCl6, Alfa Aesar) and disodium phosphate (0.250 M, Na2HPO4, Sigma-Aldrich Co. LLC.) [3].

For the deposition of the second Au layer, the pH of the plating solution was adjusted to be 11-12 by adding 4 M potassium hydroxide (KOH) aqueous solution to avoid hydrogen evolution [3]. The second Au layer was deposited at -0.95V in the beginning and then the voltage was decreased to -1.05 V. After the sequential electrochemical deposition, the silver sacrificial layer and AAO membrane were dissolved in nitric acid and 5 M sodium hydroxide aqueous solution, respectively, to disperse nanorods in DI water. MERLIN field emission scanning electron microscopy (Carl Zeiss Inc.) and energy-dispersive X-ray spectroscopy (Oxford Instruments, integrated with INCA software) were used to characterize the size and composition of tripartite rods (Fig. S1). The total rod length of $2.18 \pm 0.39\mu$m was obtained from the measurement of 200 rods.

2 Experimental methods

The motion of the rods on a polystyrene coated microscope cover slip (8% 280k PS in toluene, spin-coated at 3000 rpm for 70s) are examined using an inverted optical microscope (Nikon Eclipse TE300) with a Nikon plan apo 100× oil objective. As the rods are significantly more dense than the solution they settle to the surface of the coverslip, making the system essentially 2D. Videos of the motion are recorded at frame rates of 10.3 and 17.3 Hz and the movement is tracked using a MatLab code written for the purpose, which measures both the position and the total angle of a rod with time. An example micrograph is shown in Fig. S1d.

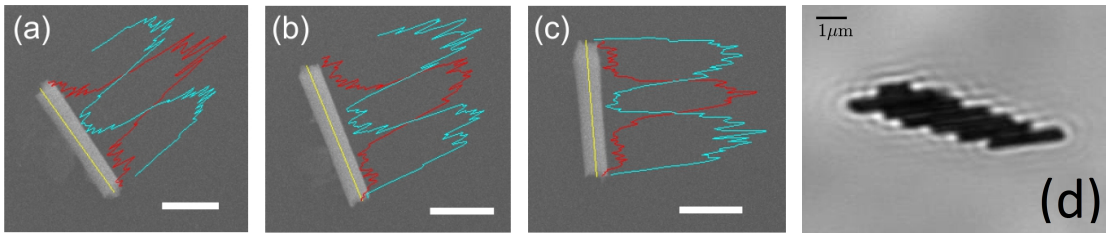

Figure S1: (a-c) Representative electron microscope images of tripartite rods overlaid with composition distribution (Au: cyan, Pt: red line). Scale bar is 1 μm. (d) Micrograph of a seven-rod rotor. Scale bar is 1 μm.

Further images and videos were taken using the same objective and a Nikon Eclipse Ti-E microscope and an Andor Zyla sCMOS camera. The results from these were not used for the analysis in Fig. 2-5. All reflection mode micrographs (Fig. 1 and movies S2 and S3) were taken using this second microscope.

3 Translational diffusion

The system of Langevin equations (Eq. 1-3 in the paper), can be solved [4, 5, 6] to find

$$\begin{aligned}\Delta R(t)^2 = \; & 4Dt + \frac{2v^2 D_r t}{D_r^2+\omega^2} + \frac{2v^2(\omega^2 - D_r^2)}{(D_r^2+\omega^2)^2} \\ & + \frac{2v^2 e^{-D_r t}}{(D_r^2+\omega^2)^2}\left((D_r^2-\omega^2)\cos(\omega t) - 2\omega D_r \sin(\omega t)\right).\end{aligned} \tag{1}$$

An average over a time series is calculated by taking every possible sample of length Δt from a time series, treating these samples as independent experiments and taking an ensemble average. For Fig. 4 in the paper $\Delta t = 1$s. Only time series which had $n_t > 10 \times n_s$, where n_t is the number of points in the time series and n_s is the number of points in a sample. An example of a fit of the full model (Eq. 1) to example data is shown in Fig. S2.

For the example shown in Fig. S2, $D_r = 0.09$ rad$^2/s$, $\omega = 6.5$ rad$/s$, $D = 0.15$ μm$^2/s$ and $v = 7$ μm$/s$. Values of D and D_r decreased with number of rods in a rotor, in keeping with the increased length of the structure. Typical values for $D = 0.21$ μm$^2/s$ for two-rod rotors and $D = 0.12$ μm$^2/s$ for three-rod rotors. Typical values for $D_r = 0.15$ rad$^2/s$ for two-rod rotors and $D_r = 0.11$ rad$^2/s$ for three-rod rotors. A typical value for $v = 2$ μm$/s$ for rotors of between two and four rods, however this varied between 0 and 7 μm$/s$.

Typical values for the rotation rate (ω) for rotors composed of 2 to 4 rods, at two different fuel concentrations (3% and 5% H_2O_2) is plotted in Fig. S3. The conductivity was not identical between the two fuel concentrations, which may account for the generally lower rotation rate of rotors at 5%, as compared to 3%.

4 Measuring stack offset

The minimum stack perimeter P_{min} occurs when the rods are fully overlapped ($\delta = 0$) and due to the geometry of a two-rod rotor, $P(t) - P_{min} = 2|\delta|$ (where P is the perimeter). Due to variation in intensity over the course of an experiment the perimeter is first normalised by the filled area of

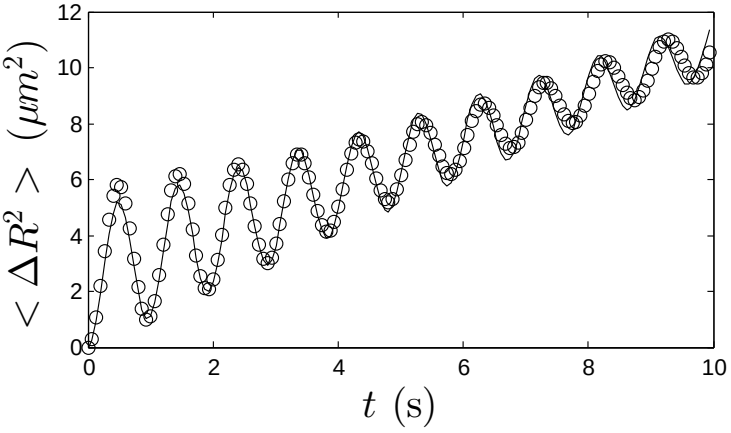

Figure S2: Example fit of Eq. 1 (solid line) to the mean squared displacement for a single rotor (o).

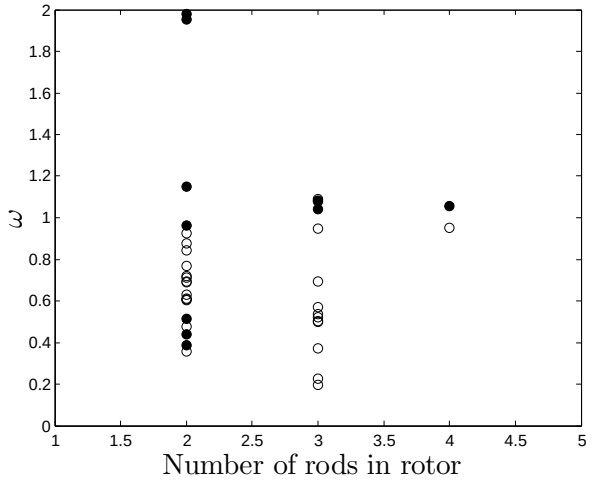

Figure S3: Rotation rate at 3% (filled circles) and 5% (open circles) H_2O_2 plotted against the number of rods in a rotor.

a stack,

$$P(t) = P^*(t) \times \sqrt{\overline{A}/A(t)}$$

where P^* is the perimeter at time t, $A(t)$ is the filled area and $\overline{A}$ is the mean filled area.

5 Supplementary Movies

All movies are in real time and should run on VLC, Windows Media Player and QuickTime.

1. *S1_single_rotor_forming.mp4*
   Shows formation of a two-rod rotor. Recorded using transmission mode.

2. *S2_rotor_switch.mp4*
   Shows a two-rod rotor switching direction. Forms a T-swimmer as the transient state. Recorded using reflection mode.

3. *S3_rotor_add_rod.mp4*
   Shows a rod being added to a three-rod rotor to create a four-rod rotor. Recorded using reflection mode.

4. *S4_T_swimmer.mp4*
   Shows a T-swimmer translating. Recorded using transmission mode.

5. *S5_transitions_between_rotor_and_tswimmer.mp4* Shows a pair of rods transitioning between T-swimmer and rotor. Recorded using transmission mode.

6. *S6_tswimmers_colliding_with_rotors.mp4* Shows various behaviours that result from a T-swimmer colliding with rotors. Recorded using transmission mode. This video is at half-speed.

References

[1] Matthew J Banholzer, Lidong Qin, Jill E Millstone, Kyle D Osberg, and Chad A Mirkin. On-wire lithography: synthesis, encoding and biological applications. *Nature protocols*, 4(6):838–848, 2009.

[2] Mordechay Schlesinger and Milan Paunovic. *Modern Electroplating: Fifth Edition*. 2011.

[3] John J. Whalen, James D. Weiland, and Peter C. Searson. Electrochemical Deposition of Platinum from Aqueous Ammonium Hexachloroplatinate Solution, 2005.

[4] Sven Van Teeffelen and Hartmut Löwen. Dynamics of a Brownian circle swimmer. *Physical Review E*, 78(2):020101, 2008.

[5] Stephen J. Ebbens, Richard Jones, Anthony Ryan, Ramin Golestanian, and Jonathan R. Howse. Self-assembled autonomous runners and tumblers. *Physical Review E*, 82(1):015304, 2010.

[6] Nathan Marine, Philip Wheat, Jesse Ault, and J. D. Posner. Diffusive behaviors of circle-swimming motors. *Physical Review E*, 87(5):052305, 2013.